

Entangling distant atom clouds through Rydberg dressing

S. Möbius, M. Genkin, A. Eisfeld, S. Wüster,^{*} and J. M. Rost

Max Planck Institute for the Physics of Complex Systems, Nöthnitzer Strasse 38, 01187 Dresden, Germany

(Received 18 December 2012; published 13 May 2013)

In Rydberg dressed ultracold gases, ground-state atoms inherit properties of a weakly admixed Rydberg state, such as sensitivity to long-range interactions. We show that through hyperfine-state-dependent interactions, a pair of atom clouds can evolve into a spin and subsequently into a spatial mesoscopic superposition state: The pair is in a coherent superposition of two configurations, with cloud locations separated by micrometers. The mesoscopic nature of the state can be proven with absorption imaging, while the coherence can be revealed through recombination and interference of the split wave packets.

DOI: [10.1103/PhysRevA.87.051602](https://doi.org/10.1103/PhysRevA.87.051602)

PACS number(s): 03.75.Gg, 32.80.Ee, 32.80.Qk, 34.20.Cf

Introduction. When and why mesoscopic objects begin to behave according to our classical intuition, as exemplified by Schrödinger's famous thought experiment [1], remains one of the fundamental questions in physics. Experimental progress to demonstrate quantum coherence in mesoscopic systems is impressive, with the recent creation of superposition states of macroscopic Josephson currents [2], ten photonic qubits [3], six atomic hyperfine qubits [4], photon coherent states [5], as well as interference of fullerenes and even large biomolecules [6], and many more [7,8].

In most of these experiments the quantum-mechanical superposition does not pertain to an intuitive classical observable taking common-sense values, such as the original “alive” or “dead” of Schrödinger's cat. Instead, the superposition typically is achieved with intrinsically quantum-mechanical degrees of freedom (hyperfine or photon number states). Realizations of position-space superpositions have been limited to small delocalization lengths (several 100 nm for Ref. [6]), the resolution of which requires sophisticated near-field interferometry. Here, we propose a mesoscopic superposition in the relative distance of two ultracold atom clouds more than 10 μm apart. The relative distances of the two superposed configurations also differ on a micrometer scale, hence the existence of the two possible cloud configurations can be revealed with direct absorption imaging and the coherence of that superposition can be proven by interference upon recombination, taking mesoscopic spatial quantum superpositions into the optically resolvable micrometer domain.

In contrast to prior proposals with ultracold or Bose-Einstein condensed atoms (e.g., Refs. [9–17]), we use Rydberg states, taking advantage of their inherently strong long-range interactions and short dynamical time scales [18,19]. The resulting internal forces [20,21] let the system turn itself from a mesoscopic superposition (cat) state of spin degrees of freedom [22,23] into a spatial cat state. In addition, Rydberg systems typically allow for an accurate control of decoherence mechanisms.

The scheme (see Fig. 1) is based on a pair of atom clouds, each containing about 20 alkali atoms, which can be in one of two hyperfine levels $|g\rangle$ and $|h\rangle$ of the atomic ground state. To induce long-range dipole-dipole interactions [18,24,25] between the clouds we weakly dress the states $|g\rangle$ and $|h\rangle$

with Rydberg states $|s\rangle$ and $|p\rangle$, respectively [26–31]. These are chosen such that each cloud is in the full dipole-blockade regime [32], where only a single Rydberg excitation per cloud is possible. However, the intercloud distance is so large that excitations in different clouds do not block each other. Such interactions can lead to collective relative motion of the clouds, with a repulsive or attractive character depending on the total hyperfine state.

To realize this scheme, we first identify a suitable effective state space and Hamiltonian for our system. We then show how to create a hyperfine state, formally already a spin cat state [23,33], in which the two clouds evolve as a coherent superposition of attractive and repulsive dynamics. After a brief dwell time, single-shot absorption images would at this stage show either the green or the red configuration in Fig. 1(b). To see the coherent character of this many-body state via interference fringes, recombination of the two configurations is finally possible with the help of an external (double-well) potential, as demonstrated at the end of this Communication.

Ultracold Rydberg dressing, dipole-dipole interactions, and blockade. Consider an assembly of $2N$ neutral atoms of mass M located at positions r_n , restricted to one dimension and confined to a double-well atom trap. Half of the atoms are localized in one of the wells, forming cloud A and the rest in the other well, forming cloud B . Near the centers of each well at $x = \pm d/2$, the potential is approximately harmonic, $V(r_n) = M\omega^2(r_n \pm d/2)^2/2$, and the atoms are initially in the Gaussian trap ground state of width $\sigma = \sqrt{\hbar/M\omega}$. We consider four essential states in ^{87}Rb atoms. Two of them are long-lived hyperfine states $|F, m_F\rangle$, namely, $|g\rangle = |1, -1\rangle$ and $|h\rangle = |2, 1\rangle$ (F is the total angular momentum and m_F the associated magnetic quantum number). The other two essential states $|\nu, l\rangle$ are Rydberg states, designated by $|s\rangle = |80, 0\rangle$ and $|p\rangle = |80, 1\rangle$ (ν is the principal quantum number and l the orbital angular momentum). The Rydberg states are coupled to the ground states with Rabi frequency Ω and detuning Δ , as sketched in Fig. 1(a). The coupling is off resonant, hence $\alpha \equiv \Omega/2\Delta \ll 1$. As shown in Ref. [29] this arrangement gives rise to effective long-range (state changing) dipole-dipole interactions of the form $D(r)(|\tilde{g}\tilde{h}\rangle\langle\tilde{g}\tilde{h}| + \text{c.c.})$, between *dressed* ground states $|\tilde{g}\rangle \sim |g\rangle + \alpha|s\rangle$, $|\tilde{h}\rangle \sim |h\rangle + \alpha|p\rangle$. We have $D(r) \approx \alpha^4 \mu^2 / r^3$, where the transition dipole μ parametrizes the strength of the bare dipole-dipole interaction. Hence, we can further reduce the essential electronic state space of a single atom to $|\tilde{g}\rangle$ and $|\tilde{h}\rangle$, on which we build

^{*}sew654@pks.mpg.de

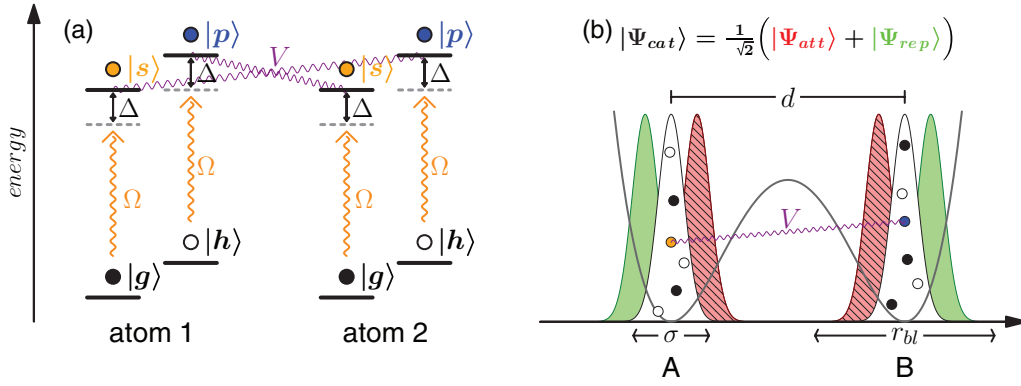


FIG. 1. (Color online) Schematic of Rydberg dressed atom clouds. (a) All atoms are in either of two hyperfine ground states $|g\rangle, |h\rangle$. Dressing lasers can couple one atom per cloud to either of the $|s\rangle, |p\rangle$ Rydberg states. The Rydberg states participate in state changing dipole-dipole interactions $|sp\rangle \leftrightarrow |ps\rangle$. (b) Two atom clouds with width σ , separated by a distance d ; r_{bl} indicates the blockade radius. Due to hyperfine-state-dependent intercloud forces, a suitable initial state evolves dynamically into a nonclassical position-space superposition state, with the pair of clouds in either the full shaded (red) or striped (green) configuration.

the many-body basis $|\mathbf{k}\rangle \equiv |k_1 \dots k_{2N}\rangle \equiv |k_1\rangle \otimes \dots \otimes |k_{2N}\rangle$, where $k_j \in \{S\} \equiv \{\tilde{g}, \tilde{h}\}$ describes the electronic state of the atom j . We formulate the many-body Hamiltonian

$$\hat{H} = \hat{H}_0 + \hat{H}_{\text{int}}, \quad \hat{H}_{\text{int}} = \sum_{n \in A, l \in B} D_{nl}(\mathbf{R}) \hat{\sigma}_{\tilde{g}\tilde{h}}^{(n)} \hat{\sigma}_{\tilde{h}\tilde{g}}^{(l)} + \text{H.c.}, \quad (1)$$

$$\hat{H}_0 = \sum_{n=1}^{2N} \left[-\frac{\hbar^2}{2M} \nabla_{r_n}^2 + V(r_n) \right],$$

with $\hat{\sigma}_{kk'}^{(n)} = |k_n\rangle\langle k'_n|$ where $k_n, k'_n \in S$ in \hat{H}_{int} , while $D_{nl}(\mathbf{R}) = D(|r_n - r_l|)$ describes the induced transition dipole-dipole interactions. Here the operator $\hat{\sigma}^{(n)}$ acts only on the Hilbert space of atom n and as unity otherwise. The vector $\mathbf{R} = \{r_1, \dots, r_{2N}\}^T$ contains all atom coordinates. Note that our model contains no interactions between two atoms in the same cloud, since the required doubly Rydberg excited intermediate state is strongly energetically suppressed through the dipole blockade, and can hence be neglected. The total number N_h of atoms in state $|\tilde{h}\rangle$ is used to classify the electronic states, since N_h is conserved by \hat{H}_{int} .

Having set up our effective state space and Hamiltonian, we can construct adiabatic Born-Oppenheimer (BO) potential surfaces $U_l(\mathbf{R})$ defined by $\hat{H}_{\text{int}}(\mathbf{R})|\varphi_l(\mathbf{R})\rangle = U_l(\mathbf{R})|\varphi_l(\mathbf{R})\rangle$ [34]. As discussed in previous work [35,36] the motion of atoms is determined by these BO potentials, as long as nonadiabatic effects are small (see also the Supplemental Material [37]). We characterize Born-Oppenheimer surfaces in the vicinity of the initial configuration sketched in Fig. 1, with the dichotomic central many-body position $\mathbf{R}_0 = (-d/2, \dots, -d/2, d/2, \dots, d/2)^T$ around which the positions of the atoms (\mathbf{R}) are randomly distributed with width σ . We choose $d = 11 \mu\text{m}$ and $\sigma = 0.5 \mu\text{m}$.

In Fig. 2(a) we show cuts through BO surfaces for states with $N_h = N$ (half of the atoms in $|\tilde{h}\rangle$) as a function of d . The insets show coefficients $c_{\mathbf{k}}$ of the two eigenstates $|\Psi_{\text{rep/att}}\rangle = \sum_{\mathbf{k}} c_{\mathbf{k}, \text{rep/att}} |\mathbf{k}\rangle$ with the largest absolute eigenvalues $U_{\text{rep/att}}(\mathbf{R}) \approx \pm N^2 D(d)/2$. These states are of particular interest, since the respective BO surfaces correspond to motion of all atoms such that one observes an attractive or

repulsive dynamics of the two clouds as entities. This can be deduced from the gradient of $U_{\text{rep/att}}$. Consequently, after preparing the twin atom clouds in a hyperfine state $|\Psi_{\text{cat}}\rangle = (|\Psi_{\text{att}}\rangle + |\Psi_{\text{rep}}\rangle)/\sqrt{2}$, one obtains a spatial superposition state as sketched in Fig. 1(b) through motional dynamics.

If our underlying basis is mapped onto a spin system [37], this process can be viewed as conversion of a collective spin state into a mesoscopic spatial superposition. The states $|\Psi_{\text{rep/att}}\rangle$ are close to coherent spin states in this picture, as sketched in Fig. 2(a). This conversion does not require external fields, but proceeds entirely through internal interactions within the system. Note that the collective cloud motion in a blockade regime crucially relies on the dressed character of the interaction. For bare dipole-dipole interactions only a single atom per cloud would be accelerated [38].

Having established the fundamental mechanisms underlying our system, we will outline how the initial hyperfine state $|\Psi_{\text{cat}}\rangle$ can be prepared, and then proceed to model spatial dynamics and interference.

Initial state creation. The first stage of assembling $|\Psi_{\text{cat}}\rangle$, starting from the simple state $|\tilde{\mathbf{g}}\rangle \equiv (|\mathbf{k}\rangle$ with $k_n = \tilde{g}, \forall n$), is to create $|\Psi_{\text{rep}}\rangle$. This can be achieved on time scales shorter than that of atomic motion by using a microwave field which couples the two hyperfine ground states so that the atom-field interaction Hamiltonian during initial state creation is [39]

$$\hat{H}_{\text{ini}}(\mathbf{R}) = \hat{H}_{\text{int}}(\mathbf{R}) + \hat{H}_{\text{rf}}, \quad (2)$$

$$\hat{H}_{\text{rf}} = \sum_n \left[\Omega_{\text{rf}}(t) \hat{\sigma}_{\tilde{g}\tilde{h}}^{(n)} / 2 + \text{H.c.} + \Delta_{\text{rf}}(t) \hat{\sigma}_{\tilde{h}\tilde{h}}^{(n)} \right].$$

When we analyze the spectrum of Eq. (2) for constant \hat{H}_{int} and Rabi frequency Ω_{rf} , as a function of microwave detuning Δ_{rf} , we see that the eigenstate $|\tilde{\mathbf{g}}\rangle$ at large negative detuning evolves continuously into $|\Psi_{\text{rep}}\rangle$ at $\Delta_{\text{rf}} = 0$. This state is adiabatically followed in Fig. 2(c), using the chirped microwave pulse shown in Fig. 2(b). The pulse avoids nonadiabatic transitions since the pulse length T_{rf} is long compared to the inverse energy gap ΔE^{-1} between the two eigenstates with the highest energy. The latter is well approximated by

$$\Delta E(t) = \sqrt{\Delta_{\text{rf}}(t)^2 + \Omega_{\text{rf}}(t)^2} + g(N)D(d), \quad (3)$$

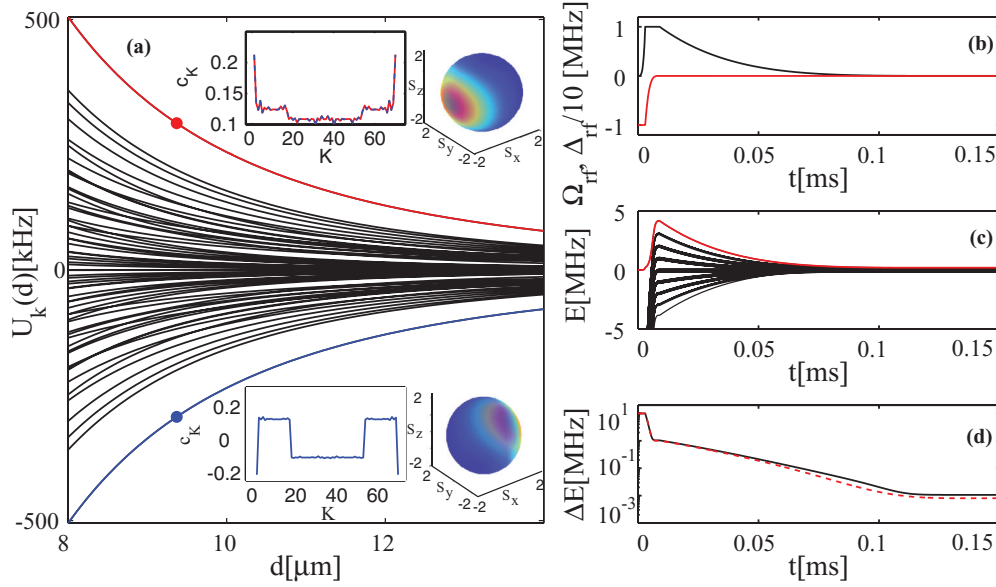


FIG. 2. (Color online) (a) Born-Oppenheimer surfaces $U_k(\mathbf{R})$ as a function of d for the case $2N = 8$, $\sigma = 1 \mu\text{m}$, $\alpha = 0.15$, and $\mu = 5760$ atomic units. Positions \mathbf{R} have been chosen around \mathbf{R}_0 in accordance with a single realization of a Gaussian distribution (width σ). The insets show the eigenstates belonging to the highest and lowest (colored) energies. Red, top inset: Coefficients $c_{\mathbf{k},\text{rep}} = \langle \mathbf{k} | \Psi_{\text{rep}} \rangle$ of the most repulsive (highest-energy) state. Blue, bottom inset: $c_{\mathbf{k},\text{att}} = \langle \mathbf{k} | \Psi_{\text{att}} \rangle$, most attractive (lowest energy). A plot of the modulus $|c_{\mathbf{k},\text{att}}|$ coincides with $c_{\mathbf{k},\text{rep}}$, since the states differ only by signs of coefficients (blue dashed, top inset). The transparent spheres visualize the Q functions of $|\Psi_{\text{rep/att}}\rangle$ in a pseudospin picture, in which the states resemble coherent spin states [37]. (b)–(d) Creation of $|\Psi_{\text{rep}}\rangle$ for $d = 11 \mu\text{m}$, using a chirped microwave pulse as described in the text. (b) Time dependence of microwave Rabi frequency Ω_{rf} (black) and detuning $\Delta_{\text{rf}}/10$ (red). (c) Resulting energy spectrum of \hat{H}_{ini} , Eq. (2), the gray (red) line, is the state to be adiabatically followed. (d) Energy gap between the two highest states of (c) (black), compared with analytical prediction Eq. (3) (red dashed).

with an only weakly N -dependent factor $g(N) \sim 0.5$, as shown in the Supplemental Material [37]. The result Eq. (3) simplifies the determination of realistic parameter regimes. We have numerically modeled the pulse of Fig. 2(b) for $2N = 8$ and found a fidelity $\mathcal{F} = |\langle \Psi_{\text{rep}} | \Psi(T_{\text{rf}}) \rangle| = 0.85$ when averaging over the atomic position distribution. Our creation scheme for $|\Psi_{\text{rep}}\rangle$ closely follows the method of [40].

The second stage of initial state creation is to convert $|\Psi_{\text{rep}}\rangle$ into $|\Psi_{\text{cat}}\rangle$. We find that $|\Psi_{\text{rep}}\rangle$ and $|\Psi_{\text{att}}\rangle$ are always related as shown in Fig. 2(a): $|\Psi_{\text{att}}\rangle$ is obtained from $|\Psi_{\text{rep}}\rangle$ by a π phase shift to every coefficient of basis states involving an odd number N_{hA} of atoms in $|\hbar\rangle$ in cloud A. By applying this phase shift conditional on some control atom in a $(|0\rangle + |1\rangle)/\sqrt{2}$ superposition we achieve our goal. This can be realized precisely as in a recent proposal for mesoscopic Rydberg quantum computation gates [41] (see also Refs. [22,37]). When modeling this final step of the initial state creation sequence, we find that fidelity loss is negligible compared to the one incurred in the previous stage of creating $|\Psi_{\text{rep}}\rangle$. This situation should persist for larger N [41]. The initial state creation sequence just described is additionally robust against fluctuations of atom numbers [37,42,43].

Spatial superposition state and interference. To turn the electronic state $|\Psi_{\text{cat}}\rangle$ prepared so far into a mesoscopic spatial superposition, we keep the dressed interactions switched on for an acceleration period $\tau_{\text{acc}} \sim 6 \mu\text{s}$, after which they are adiabatically switched off to avoid spontaneous decay of the Rydberg population. After mechanical evolution in the trap for a time $\tau_{\text{trap}}/4 = \pi/(2\omega)$, the clouds reach their maximal displacement, where the macroscopic spatial superposition

character of the quantum state can be shown with μm resolution atom detection. An absorption image would always show two inert clouds, with a 50% probability at either of the two configurations marked I and O in Fig. 3. If instead the spatial dynamics is allowed to proceed until time $\tau_{\text{trap}}/2$ where the spatial wave function recombines and all atoms are reunited in the same hyperfine state [44], the absorption image will show an interference pattern, demonstrating the coherence of the superposition.

We solve the Schrödinger equation as in Refs. [35,37,45] to model the quantum dynamics of acceleration, splitting, and recombination for $2N = 4$ in a plane-wave basis and for $2N = 6$ in a Hermite-Gauss basis. Interference fringes develop in the probability distribution $\rho(z)$ of the relative intercloud distance $\hat{z} = (\sum_{n \in A} \hat{R}_n - \sum_{n \in B} \hat{R}_n)/N$. We extract $\rho(z)$ from the many-body wave function as $\rho(z, t) = \int \overline{dR} |\Psi(\mathbf{R}, t)|^2$, where $\int \overline{dR}$ denotes integration over all coordinates orthogonal to z . At $t = \tau_{\text{trap}}/2$, we find full contrast interference fringes in both cases. We thus believe that they persist also for larger atom numbers, as no new physics enters beyond three atoms per cloud. Atomic densities and interference for $2N = 4$ are shown in Fig. 3, which additionally includes results obtained with Tully's quantum-classical algorithm [20,36,46], with which slightly larger atom numbers can be treated (~ 8 – 12). We find that nonadiabatic effects during the acceleration phase are negligible, with a population loss of $P_{na} = 1 - p_{\text{rep}} = 10^{-9}$ out of the target state $|\Psi_{\text{cat}}\rangle$ for the situation of Fig. 3. For larger N the situation improves further.

While computational demands limit the simulations shown to $2N \leq 6, 8$ we extrapolate that spatial cat states are realistic

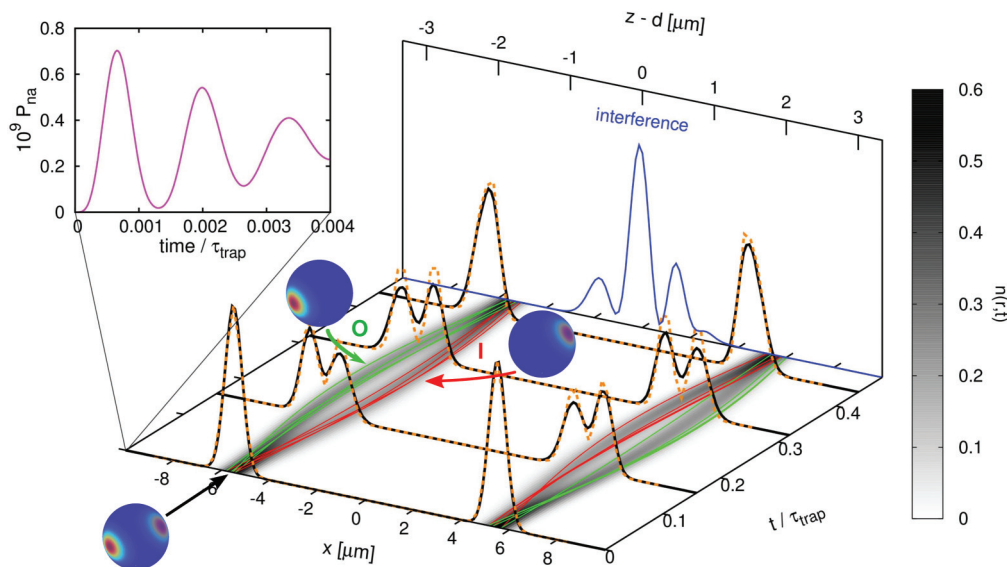


FIG. 3. (Color online) Evolution of the initial hyperfine state $|\Psi_{\text{cat}}\rangle$ into a spatial superposition of cloud locations for $2N = 4$ and trap frequency $\omega = (2\pi) \times 400$ Hz. We compare the total atomic density $n(x, t)$ from quantum-classical simulations (gray shading, black three-dimensional lines), to full quantum solutions (orange dashed). The lines overlaid on the gray shading are exemplary repulsive, marked O (green), and attractive, marked I (red), quantum-classical trajectories. Transparent spheres show the conversion of a spin cat state into a spatial cat state that would underlie this process for $N = 20$, spin coordinate axes for spheres as in Fig. 2. Nonadiabatic population loss P_{na} from $|\Psi_{\text{cat}}\rangle$ during the initial acceleration phase is shown magnified in the left inset (magenta). The back panel shows the interference signal found in the relative distance distribution $\rho(z)$ at $t = \tau_{\text{trap}}/2$ (blue); note the different abscissa used.

for up to $N = 20$ for the parameters used in this Rapid Communication. Nonadiabatic effects during acceleration and initial state creation are under control for larger N . The main limitation comes from the lifetime of the Rydberg states used for the dressing, since just a single decay has the potential to destroy the fragile cat state. However, we can choose parameters for which the probability of even a single decay is small. This is for example achieved for $d = 11 \mu\text{m}$, $\sigma = 0.5 \mu\text{m}$, $\alpha = 0.15$, assuming ^{87}Rb atoms with $\nu = 80$. We use $\mu = \mu_0 v^2$, where $\mu_0 = 0.97$ a.u. for ^{87}Rb . The overall lifetime of the system under dressing interactions is $\tau_{\text{life}} = \tau/(2N)$, with $\tau = \tau_0/\alpha^2$ and $\tau_0 = 209.42 \mu\text{s}$ [47]. For our parameters $\tau_{\text{life}} = 0.23$ ms, larger than the time required for initial state creation (0.15 ms) and acceleration (6 μs).

Conclusion. We have proposed a setup in which two cold atom clouds of about 20 atoms each evolve dynamically by internal forces into a spatial mesoscopic quantum superpo-

sition state if exposed to Rydberg dipole-dipole interactions through dressing. The interactions create a state where two entire atomic clouds simultaneously are at two quantum-mechanically superimposed locations, which are macroscopically distinguishable. Hence they can be resolved by visible light.

The internal forces that induce motion of the atomic clouds are also instrumental in creating the required intermediate hyperfine state $|\Psi_{\text{rep}}\rangle$. This state may have interesting applications by itself due to its entanglement structure between the two clouds. Finally, the hyperfine state $|\Psi_{\text{rep}}\rangle + |\Psi_{\text{att}}\rangle$ prior to any spatial dynamics realizes a collective spin superposition state.

Acknowledgments. We gladly acknowledge fruitful discussions with Igor Lesanovsky, Klaus Mølmer, Markus Müller, Pierre Pillet, Thomas Pohl, and Shannon Whitlock, and EU financial support received from the Marie Curie Initial Training Network (ITN) “COHERENCE.”

- [1] E. Schrödinger, *Naturwissenschaften* **23**, 807 (1935).
- [2] J. R. Friedman, V. Patel, W. Chen, S. K. Tolpygo, and J. E. Lukens, *Nature (London)* **406**, 43 (2000).
- [3] W.-B. Gao *et al.*, *Nat. Phys.* **6**, 331 (2010).
- [4] D. Leibfried *et al.*, *Nature (London)* **438**, 639 (2005).
- [5] H. Takahashi *et al.*, *Phys. Rev. Lett.* **101**, 233605 (2008).
- [6] S. Gerlich *et al.*, *Nat. Commun.* **2**, 263 (2011).
- [7] C.-Y. Lu *et al.*, *Nat. Phys.* **3**, 91 (2007).
- [8] C. Monroe, D. M. Meekhof, B. E. King, and D. J. Wineland, *Science* **272**, 1131 (1996).
- [9] C. Weiss and Y. Castin, *Phys. Rev. Lett.* **102**, 010403 (2009).
- [10] A. I. Streltsov, O. E. Alon, and L. S. Cederbaum, *J. Phys. B: At. Mol. Opt. Phys.* **42**, 091004 (2009).
- [11] N. Bar-Gill, D. D. Bhaktavatsala Rao, and G. Kurizki, *Phys. Rev. Lett.* **107**, 010404 (2011).
- [12] J. I. Cirac, M. Lewenstein, K. Mølmer, and P. Zoller, *Phys. Rev. A* **57**, 1208 (1998).
- [13] D. A. R. Dalvit, J. Dziarmaga, and W. H. Zurek, *Phys. Rev. A* **62**, 013607 (2000).
- [14] J. A. Dunningham, K. Burnett, R. Roth, and W. D. Phillips, *New J. Phys.* **8**, 182 (2006).
- [15] D. Gordon and C. M. Savage, *Phys. Rev. A* **59**, 4623 (1999).

- [16] D. W. Hallwood, T. Ernst, and J. Brand, *Phys. Rev. A* **82**, 063623 (2010).
- [17] H. T. Ng, *Phys. Rev. A* **77**, 033617 (2008).
- [18] T. F. Gallagher, *Rydberg Atoms* (Cambridge University Press, Cambridge, UK, 1994).
- [19] M. Saffman, T. G. Walker, and K. Mølmer, *Rev. Mod. Phys.* **82**, 2313 (2010).
- [20] S. Wüster, C. Ates, A. Eisfeld, and J. M. Rost, *Phys. Rev. Lett.* **105**, 053004 (2010).
- [21] C. Ates, A. Eisfeld, and J. M. Rost, *New J. Phys.* **10**, 045030 (2008).
- [22] M. Saffman and K. Mølmer, *Phys. Rev. Lett.* **102**, 240502 (2009).
- [23] T. Opatrný and K. Mølmer, *Phys. Rev. A* **86**, 023845 (2012).
- [24] W. Li, P. J. Tanner, and T. F. Gallagher, *Phys. Rev. Lett.* **94**, 173001 (2005).
- [25] A. Fioretti, D. Comparat, C. Drag, T. F. Gallagher, and P. Pillet, *Phys. Rev. Lett.* **82**, 1839 (1999).
- [26] L. Santos, G. V. Shlyapnikov, P. Zoller, and M. Lewenstein, *Phys. Rev. Lett.* **85**, 1791 (2000).
- [27] N. Henkel, R. Nath, and T. Pohl, *Phys. Rev. Lett.* **104**, 195302 (2010).
- [28] G. Pupillo, A. Micheli, M. Boninsegni, I. Lesanovsky, and P. Zoller, *Phys. Rev. Lett.* **104**, 223002 (2010).
- [29] S. Wüster, C. Ates, A. Eisfeld, and J. M. Rost, *New J. Phys.* **13**, 073044 (2011).
- [30] F. Maucher, N. Henkel, M. Saffman, W. Królikowski, S. Skupin, and T. Pohl, *Phys. Rev. Lett.* **106**, 170401 (2011).
- [31] J. E. Johnson and S. L. Rolston, *Phys. Rev. A* **82**, 033412 (2010).
- [32] D. Jaksch, J. I. Cirac, P. Zoller, S. L. Rolston, R. Côté, and M. D. Lukin, *Phys. Rev. Lett.* **85**, 2208 (2000).
- [33] J. Ma, X. Wang, C. P. Sun, and F. Nori, *Phys. Rep.* **509**, 89 (2011).
- [34] W. Domcke, D. R. Yarkony, and H. Köppel, *Conical Intersections* (World Scientific, Singapore, 2004).
- [35] S. Wüster, A. Eisfeld, and J. M. Rost, *Phys. Rev. Lett.* **106**, 153002 (2011).
- [36] S. Möbius, S. Wüster, C. Ates, A. Eisfeld, and J. M. Rost, *J. Phys. B: At. Mol. Opt. Phys.* **44**, 184011 (2011).
- [37] See Supplemental Material at <http://link.aps.org/supplemental/10.1103/PhysRevA.87.051602> for details on Born-Oppenheimer separation, spin analogy, initial state creation, and fringe visibility.
- [38] S. Möbius, M. Genkin, S. Wüster, A. Eisfeld, and J.-M. Rost, [arXiv:1212.1267](https://arxiv.org/abs/1212.1267).
- [39] The microwave couples to the bare ground states. Due to the separate time scales of bare dipole interactions $V \sim 29$ MHz, Rydberg dressing $\Omega \sim 7.5$ MHz, and microwave coupling $\Omega_{\text{rf}} \sim 1$ MHz, we expect that it adiabatically manipulates dressed states and write Eq. (2) directly in terms of dressed ground states $|\tilde{g}\rangle, |\tilde{h}\rangle$.
- [40] T. Pohl, E. Demler, and M. D. Lukin, *Phys. Rev. Lett.* **104**, 043002 (2010).
- [41] M. Müller, I. Lesanovsky, H. Weimer, H. P. Büchler, and P. Zoller, *Phys. Rev. Lett.* **102**, 170502 (2009).
- [42] A. M. Dudarev, M. G. Raizen, and Q. Niu, *Phys. Rev. Lett.* **98**, 063001 (2007).
- [43] C. Chuu, F. Schreck, T. P. Meyrath, J. L. Hanssen, G. N. Price, and M. G. Raizen, *Phys. Rev. Lett.* **95**, 260403 (2005).
- [44] E.g., by using a second chirped microwave pulse to transfer all atoms to $|g\rangle$; dressed interactions can remain off.
- [45] The SE and Tully's algorithm were both implemented in the high-level simulation language XMDS [48,49].
- [46] J. C. Tully, *J. Chem. Phys.* **93**, 1061 (1990).
- [47] I. I. Beterov, I. I. Ryabtsev, D. B. Tretyakov, and V. M. Entin, *Phys. Rev. A* **79**, 052504 (2009).
- [48] G. R. Dennis, J. J. Hope, and M. T. Johnsson, *Comput. Phys. Commun.* **184**, 201 (2013).
- [49] G. R. Dennis, J. J. Hope, and M. T. Johnsson, <http://www.xmds.org/>.